MAUSAM, **74**, 3 (July 2023), 561-578

MAUSAM

DOI : https://doi.org/10.54302/mausam.v74i3.5112
Homepage: https://mausamjournal.imd.gov.in/index.php/MAUSAM

UDC No. 551.509.313 : 551.573 (545.2)

Modeling medium resolution evapotranspiration using downscaling techniques in north-western part of India

ARVIND DHALOIYA, DARSHANA DUHAN*[@], D. M. DENIS**, DHARMENDRA SINGH***, MUKESH KUMAR* and MANENDER SINGH*[#]

Department of Soil and Water Engineering, PAU, Ludhiana, Punjab, India

**Department of Soil and Water Engineering, CCS HAU, Hisar, Haryana, India*

***Department of Irrigation and Drainage Engineering, VIAET, SHUATS, Prayagraj, UP, India*

****Haryana Space Applications Centre (HARSAC), Hisar, Haryana, India*

**[#]Department of Horticulture, CCS HAU, Hisar, Haryana, India*

(*Received 20 January 2022, Accepted 12 December 2022*)

[@]**e mail : darshuduhan2@gmail.com**

सार — वर्तमान जांच डाउनस्केलिंग मॉडल को नियोजित करके मौसम संबंधी और लैंडसैट 8 (ऑपरेशनल लैंड इमेजर, ओएलआई) डेटा का उपयोग करके अपने मूल 500 एम एसस्पेशियल रिज़ॉल्यूशन से 30 मीटर स्थानिक रिज़ॉल्यूशन पर डाउनस्केल मोडिस-आधारित वाष्पीकरण (ईटी) के लिए एक मॉडलिंग समाधान प्रदान करता है। सतह अल्बेडो, भूमि सतह तापमान (LST), सामान्यीकृत अंतर वनस्पति सूचकांक (NDVI), मृदा-समायोजित वनस्पति सूचकांक (SAVI), संशोधित मृदा-समायोजित वनस्पति सूचकांक (MSAVI), सामान्यीकृत अंतर निर्मित सूचकांक (NDBI) नामक नौ सूचकांक।, सामान्यीकृत अंतर जल सूचकांक (एनडीडब्ल्यूआई), सामान्यीकृत अंतर नमी सूचकांक (एनडीएमआई), और बैंड 7 (एनडीआईआईबी7) के लिए सामान्यीकृत अंतर इन्फ्रारेड सूचकांक की गणना लैंसेट 8 डेटा से 30 मीटर स्थानिक विभेदन पर की गई थी। 500 मीटर पैमाने पर MODIS 500 मीटर ET और लैंडसैट सूचकांकों के बीच संबंध उत्पन्न करने के लिए मल्टीपल लीनियर रिग्रेशन (MLR) और लीस्ट स्क्वायर सपोर्ट वेक्टर मशीन (LS-SVM) मॉडल विकसित किए गए थे। इसके अलावा, इन विकसित मॉडलों का उपयोग 30 मीटर लैंडसैट 8 सूचकांकों के आधार पर 30 मीटर ईटी का अनुमान लगाने के लिए किया गया था। विकसित मॉडल (MLR और LS-SVM) का प्रदर्शन सहसंबंध गुणांक (CC), नैश-सटक्लिफ गुणांक (NASH) दक्षता, रूट मीन स्क्वायर एरर (RMSE) और नॉर्मलाइज़्ड मीन स्क्वायर एरर (NMSE) का उपयोग करके किया गया था। पेनमैन-मॉंटिथ (पीएम) पद्धति का उपयोग प्रेक्षित स्टेशन डेटा का उपयोग करके ईटी का अनुमान लगाने के लिए किया गया था। परिणाम बताते हैं कि दिसंबर के महीने में सबसे कम ईटीओ देखा गया जबकि मई के महीने में यह अधिकतम था। प्रदर्शन सूचकांकों का उपयोग करते हुए, यह पाया गया कि एलएस-एसवीएम मॉडल ने एमएलआर मॉडल की तुलना में थोड़ा बेहतर प्रदर्शन किया। हालांकि, डाउनस्केल्ड मॉडल पेनमैन-मॉंटिथ पद्धति की तुलना में ईटी को अधिक आंकता है। इसके अलावा, सभी स्टेशनों पर MODIS ET और LS-SVM ET के बीच महत्वपूर्ण सहसंबंध पाया गया।

ABSTRACT. The present investigation provides a modeling solution to downscale MODIS-based evapotranspiration (ET) at a 30 m spatial resolution from its original 500 m spatial resolution using meteorological and Landsat 8 (Operational Land Imager, OLI) data by employing downscaling models. The nine indices namely Surface Albedo, Land Surface Temperature (LST), Normalized Difference Vegetation Index (NDVI), Soil-Adjusted Vegetation Index (SAVI), Modified Soil-Adjusted Vegetation Index (MSAVI), Normalized Difference Built-up Index (NDBI), Normalized Difference Water Index (NDWI), Normalized Difference Moisture Index (NDMI) and Normalized Difference Infrared Index for Band 7 (NDIIB7) were calculated from Lansat 8 data at 30 m spatial resolution. The multiple linear regression (MLR) and Least Square Support Vector Machine (LS-SVM) models were developed to generate the relationship between MODIS 500 m ET and Landsat indices at 500 m scale. Further, these develop models were used to estimate 30 m ET based on 30 m Landsat 8 indices. The performance of developed models (MLR and LS-SVM) was carried out using correlation coefficient (CC), Nash-Sutcliffe coefficient (NASH) efficiency, Root Mean

Square Error (RMSE) and Normalised Mean Square Error (NMSE). Penman-Monteith (PM) method was used to estimate the ET using observed station data. The results show that lowest ETO was observed in the month of December while it was maximum in the month of May. Using the performances indices, it was found that LS-SVM model slightly out performed than MLR model. However, the downscaled model overestimates ET in comparison to the Penman-Monteith method. Further, the significant correlation was found between MODIS ET and LS-SVM ET at all the stations.

Key words – Downscaling, Evapotranspiration, MODIS, Landsat, MLR, LS-SVM.

1. Introduction

Evapotranspiration (ET) which is the sum of evaporation from soil and transpiration from trees is considered to be an important component of the ecosystem function (Hansen *et al*., 1980) and its rate depends on many variables like solar radiation, temperature, wind velocity, moisture and specific vegetation characteristics, which can vary considerably between types of vegetation (Allen *et al*., 1998). The spatial and temporal assessment of ET is needed for drought monitoring, ecosystem health assessment, water requirement estimation and agricultural water allocation and management at local to regional scales (Anderson *et al*., 2012; Duhan *et al*., 2021).

The various models were developed to estimate ET like through physical (*i.e*., evaporation pans), empirical (*i.e*., temperature-based (Thornthwaite, 1948 Blaney & Criddle 1950; Hargreaves & Samani 1985), radiation-based (Priestley & Taylor 1972); combination of both (Penman 1948; Monteith 1965) and satellite-based (Moderate Resolution Imaging Spectroradiometer; MODIS). Among the empirical based method, Penman-Monteith method (Allen *et al*., 1998) is successfully used to calculate reference evapotranspiration (ET_0) under different climatic conditions (Goyal 2004; Jhajharia *et al*., 2012). In recent decades various soft computing techniques (*e.g*., artificial neural networks, fuzzy and neuro-fuzzy systems, support vector machine and genetic algorithms) are also applied successfully for modelling the ET around the world (Duhan *et al*., 2021; Niaghi *et al*., 2021; Yang *et al*., 2021; Yao *et al*., 2017; Wang *et al*., 2017). Yang *et al*. (2021) used Bayesian model averaging (BMA) method with eight ET models (*i.e*., four surface energy balance models (*i.e*., SEBS, SEBAL, SEBI, and SSEB) and four machine learning algorithms (*i.e*., polymars, random forest, ridge regression, and support vector machine) to produce ET with Landsat 8 satellite data. They reported that BMA method coupled with machine learning can significantly improve the accuracy of daily ET estimate and reduce uncertainties among models. Duhan *et al*. (2021) evaluated the performance of various PET methods like pans evaporation, PM, Hargreaves, Thornthwaite and satellite-based (MODIS). They found that MOD16 and Hargreaves methods overestimate the PET; however, the PM and Thornwaite methods underestimate the PET in comparison to ET pan in the semiarid region. Further they also concluded that PM-based PET is closely related with ETpan and it is a good indicator of ETpan in a semiarid region. The fuzzy genetic and least square support vector regression (LS-SVR) models with more input variables perform better than the MARS, M5Tree and MLR models in predicting ETpan in the Dongting Lake Basin, China (Wang *et al*., 2017). Niaghi *et al*. (2021) reported that RF model illustrated the best performance among the Gene Expression Programming (GEP), Support Vector Machine (SVM), Multiple Linear Regression (LR) and Random Forest (RF) models to estimate ET_0 in the Red River Valley, USA.

However, due to the heterogeneity of the landscape and the complexity of biophysical processes of plants, the ET remains difficult to measure without the consideration of spatial and temporal diversity of biological parameters, such as leaf area index (LAI), normalized difference vegetation index (NDVI), albedo and etc. (Yao *et al*., 2017; Devendra *et al*., 2019, 2021). Remote sensing provides a broad spatial coverage and regular sampling of biophysical parameters (*e.g*., vegetation indices, VIs, albedo, leaf area index, LAI, fraction of absorbed photosynthetically active radiation, FPAR, land surface temperature, LST and plant functional types, PFTs) for estimating regional ET (Liang *et al*., 2013). The retrieval of ET from satellite remote sensing is an emerging tool. MOD16 PET may be a better option to estimate monthly ET in the semiarid area after applying the monthly correction factor, even when the weather stations do not have full datasets (Duhan *et al*., 2021). Yao *et al*. (2017) reported that SVM method provides a powerful tool for improving global ET estimation by integrating three process-based ET algorithms: MOD16, PT-JPL (Priestley-Taylor-Based ET algorithm) and Semi-PM (Semi-empirical Penman algorithm). Knipper *et al*. (2017) found that Moderate Resolution Imaging Spectroradiometer (MODIS) soil moisture ET overestimates annual ET when compared with eddy covariance stations data in a semiarid region of the southwest America. Mahour *et al.* (2017) used satellite data and climate data to estimate actual evapotranspiration using downscaling technique. Downscaling from MODIS to Landsat scale could be a completely beneficial method for combining the benefits of high temporal and spatial resolutions (Hong *et al*., 2011).

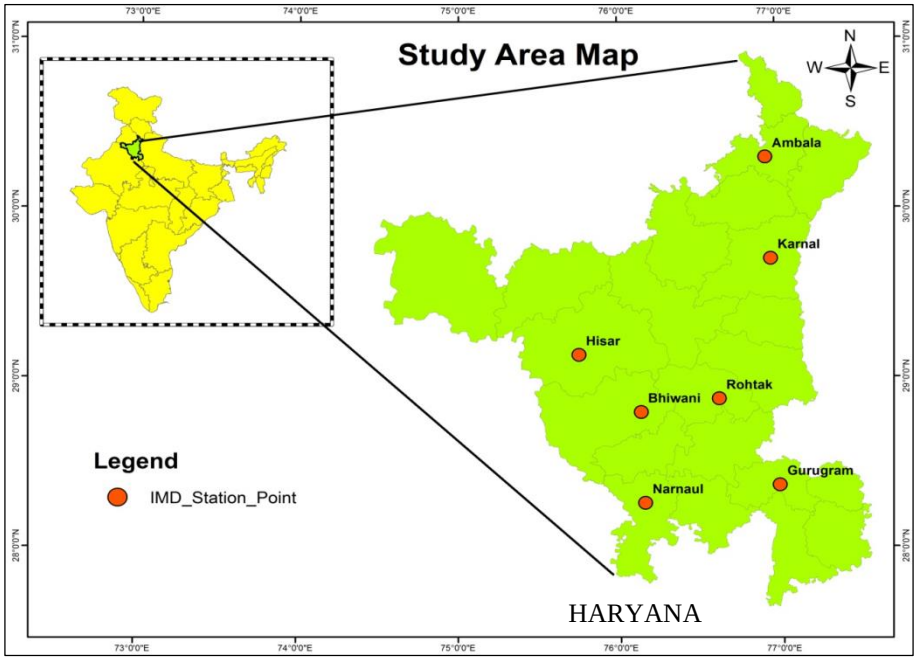

Fig. 1. Location map of study area

TABLE 1

Location of stations and meteorological parameters characteristics during the years of 2013-2018

Station Name	Lat. (°N)	Long. (°E)	Altitude at mean sea level (m)	*T*max (°C)	*T*min (°C)	Rainfall (mm/day)	ETpan (mm/day)	Wind speed (km/h)	Relative Humidity (%)	Solar radiation (MJ/m^2/day)
Ambala	30.22	76.46	274	39.76	1.61	2.56	3.8	2.92	75.02	31.42
Karnal	29.41	76. 58	249	44.55	1.46	2.48	3.96	2.76	75.18	31.59
Hisar	29.11	75.43	215	47.04	1.00	1.10	4.16	2.57	73.40	31.75
Narnaul	28.03	76.06	309	45.45	1.41	1.11	4.46	2.44	49.80	31.99
Rohtak	28.54	76.34	239	46.74	1.69	1.26	4.43	2.94	59.55	31.82
Bhiwani	28.47	76.08	223	46.31	1.00	1.76	4.05	2.36	60.59	31.84
Gurugram	28.29	76.59	214	46.06	2.35	1.92	4.36	2.54	56.15	31.96

The downscaling techniques using geostatistical model convert a low spatial resolution image into a high spatial resolution image while maintaining the radiometric properties of the image (Aiazzi *et al*., 2002). Ke *et al*. (2016) proposed a machine learning-based method to downscale MODIS ET at 30 m resolution from 1 km resolution with Landsat 8 data-derivatives and found the potential of using machine learning approaches for ET downscaling. Such a downscaled high-resolution products are essentially required for the local agriculture water management, irrigation scheduling, and monitoring water budget (Tan *et al*., 2017). However, the downscaled ET products have still not been developed for the currently taken study area. Nevertheless, this is a much-needed input for water management in this area, being fully dependent on irrigation and agriculturally intense landscape.

Looking to the aforesaid, the present study has been carried out to produce a 30 m ET product from 500 m MODIS ET(MOD16A2) and Landsat 8 data by employing Machine learning & Multiple linear regression models.

2. Study area and data

2.1. Study *area*

In the present study, Haryana State of India was selected which lies between 27° 39' 20" to 30° 55' 05" N Latitude and 74° 27' 08" to 77° 36' 05" E Longitude

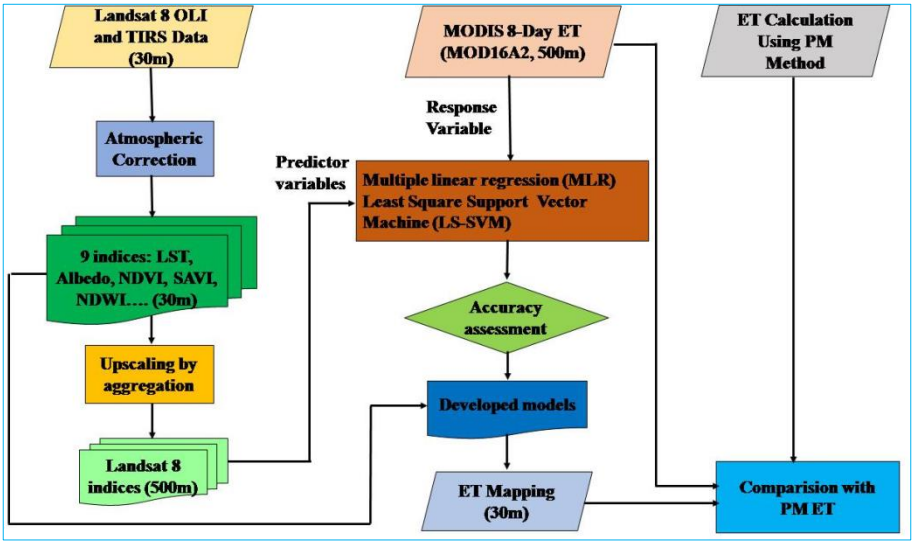

Fig. 2. Flowchart of methodology adopted in present research work

TABLE 2

Details of Landsat 8 data used in the study area

Month, Year	Data Acquisition Date	Month, Year	Data Acquisition Date
May, 2013	13/05/2013, 20/05/2013, 27/05/2013	May, 2016	19/05/2016, 21/05/2016, 28/05/2016
November, 2013	03/11/2013, 12/11/2013, 21/11/2013	June, 2016	04/06/2016, 06/06/2016, 13/06/2016
November, 2014	06/11/2014, 15/11/2014, 24/11/2014	October, 2016	12/10/2016, 19/10/2016, 26/10/2016
December, 2014	01/12/2014, 08/12/2014, 10/12/2014	March, 2017	05/03/2017, 12/03/2017, 19/03/2017
April, 2015	15/04/2015, 17/04/2015, 24/04/2015	September, 2017	20/09/2017, 27/09/2017, 29/09/2017
May, 2015	17/05/2015, 19/05/2015, 26/05/2015	October, 2017	06/10/2017, 13/10/2017, 15/10/2017
September, 2015	06/09/2015, 08/09/2015, 15/09/2015	December, 2017	02/12/2017, 09/12/2017, 16/12/2017
October, 2015	08/10/2015, 10/10/2015, 17/10/2015	March, 2018	06/03/2018, 08/03/2018, 31/03/2018

The Landsat-8 sensor provides 30-meter resolution data with 11 bands

(Fig. 1). The area is situated in the northwest part of India. The total geographical area of Haryana is 44212 km^2. The climate in the study area is arid to semi-arid. In summer, it is extremely hot at about 45°C (Singh *et al*., 2010) and in winter it is mild to very cool. May & June are the warmest months and December & January are the coldest months. The average precipitation in the study area is around 615.6 mm out of which around 80% of the precipitation is received in the monsoon seasons (from June to September) and the remaining precipitation is received in non-monsoon season (December to February) (Singh *et al.*, 2010). Haryana is primarily an agricultural State and around 70% of residents is engaged in agriculture. Agriculture and related industries are the backbone of the local economy. Wheat and rice are the major crops. Haryana is self-sufficient in food production and the second largest contributor to India's central pool of food grains (Darshana and Ashish, 2012). Northernmost part of the state is covered by forest, while southernmost part is desert and hills of Aravalli.

2.2. *Details of data*

In the present study, space-borne (satellites) and station based meteorological data were used. The meteorological data consisting of temperature (maximum and minimum), relative humidity and wind speed of seven stations namely Ambala, Bhiwani, Gurugram, Hisar, Karnal, Narnaul and Rohtak were obtained from India Meteorological Department (IMD) Pune during the year 2000 to 2018. The location of stations and characteristics of meteorological parameters were shown in Table 1. The

TABLE 3

Details of MODIS ET data used in the study area

Month, year	Data Acquisition Date	Day of the year	Month, year	Data Acquisition Date	Day of the year
May, 2013	01/05/2013, 09/05/2013	121	May, 2016	08/05/2016	129
	17/05/2013	129		16/05/2016	137
	25/05/2013	137		24/05/2016	145
		145			
November, 2013	01/11/2013	305	June, 2016	01/06/2016	153
	09/11/2013	313		09/06/2016	161
	17/11/2013	321		17/06/2016	169
	25/11/2013	329		25/06/2016	177
November, 2014	01/11/2014	305	October, 2016	07/10/2016	281
	09/11/2014	313		15/10/2016	289
	17/11/2014	321		23/10/2016	297
	25/11/2014	329		31/10/2016	305
December, 2014	03/12/2014	337	March, 2017	06/03/2017	65
	11/12/2014	345		14/03/2017	73
	19/12/2014 27/12/2014	353		22/03/2017 30/03/2017	81
		361			89
April, 2015	07/04/2015	97	September, 2017	06/09/2017	249
	15/04/2015	105		14/09/2017	257
	23/04/2015	113		22/09/2017	265
				30/09/2017	273
May, 2015	01/05/2015 09/05/2015	121	October, 2017	08/10/2017	281
	17/05/2015	129		16/10/2017	289
	25/05/2015	137		24/10/2017	297
		145			
September, 2015	06/09/2015	249	December, 2017	03/12/2017	337
	14/09/2015	257		11/12/2017	345
	22/09/2015	265		19/12/2017 27/12/2017	353
	30/09/2015	273			361
October, 2015	08/10/2015	281	March, 2018	06/03/2018	65
	16/10/2015	289		14/03/2018	73
	24/10/2015	297		22/03/2018	81
				30/03/2018	89

Landsat8 datasets (at 30 m resolution) of different row and path of the study area (Path 146/Row 40, Path 146/Row 41, Path 147/Row 39, Path 147/Row 40, Path 147/Row 41, Path 148/Row 39 and Path 148/Row 40) was downloaded from http://earthexplorer.usgs.gov/ on different dates as shown in Table 2. Further, the MODIS ET data (MOD16A2) at 500 m resolution for 8-day intervals is downloaded from the Land Processes Distributed Active Archive Center of the National Aeronautics and Space Administration (NASA) (https://lpdaac.usgs.gov/lpdaac/get_data) for all the stations in the study area (Table 3). The selected months in a particular year is purely based on availability of cloud-free image of Landsat data during the study period.

3. Methodology adopted

Fig. 2 shows the methodology adopted in the present research work. Firstly, Landsat 8 (Operational Land Imager, OLI) data were processed for the estimation of nine indices (Table 4) namely Surface Albedo, Land Surface Temperature (LST), Normalized Difference Vegetation Index (NDVI), Soil-Adjusted Vegetation Index (SAVI), Modified Soil-Adjusted Vegetation Index

TABLE 4

Formula used for the estimation of vegetation indices in the study area

S. No.	Vegetation Index	Formula	Description	Reference
1.	Land Surface Temperature (LST)	$\mathrm{LST} = \frac{BT}{1+\left[\gamma(BT) * \frac{ln(\varepsilon)}{\rho}\right]}$	BT=brightness temperature of band 10, ε = emissivity, ρ = 1.438*10^{-2} m K	Barsi *et al*.,2014
2.	Normalized Difference Vegetation Index (NDVI)	$\frac{\mathrm{NIR}-\mathrm{R}}{\mathrm{NIR}+\mathrm{R}}$	NIR is the reflectance at near-infrared spectral region and R is the reflectance at red spectral region	Rause *et al*. (1974)
3.	Soil-Adjusted Vegetation Index (SAVI)	$\frac{\mathrm{NIR}-\mathrm{R}}{\mathrm{NIR}+\mathrm{R}+\mathrm{L}} \times (1+L)$	NIR is the reflectance at near-infrared spectral region and R is the reflectance at red spectral region and L = 0.5	Huete, A. R. (1988)
4.	Modified Soil-Adjusted Vegetation Index (MSAVI)	$\mathrm{MSAVI} = \frac{\left[2*\mathrm{NIR}+1-\sqrt{(2*\mathrm{NIR}+1)^2-8*(\mathrm{NIR}-\mathrm{RED})}\right]}{2}$	NIR is the reflectance at near-infrared spectral region and RED is the reflectance at red spectral region and L = 0.5	Qi *et al*. (1994)
5.	Normalized Difference Built-up Index (NDBI)	$\frac{(\mathrm{SWIR}-\mathrm{NIR})}{(\mathrm{SWIR}+\mathrm{NIR})}$	SWIR is the reflectance at short wave near-infrared spectral region and NIR is the reflectance at Near Infra-red spectral region	Zha *et al*. (2003)
6.	Normalized Difference Water Index (NDWI)	$\frac{(\mathrm{Green}-\mathrm{NIR})}{(\mathrm{Green}+\mathrm{NIR})}$	Green is the reflectance at green spectral region and NIR is the reflectance at Near Infra-red spectral region	McFeeters (1996)
7.	Normalized Difference Moisture Index (NDMI)	$\frac{(\mathrm{NIR}-\mathrm{SWIR1})}{(\mathrm{NIR}+\mathrm{SWIR1})}$	Do	Wilson and Sader (2002)
8.	Normalized Difference Infrared Index for Band 7 (NDIIB7)	$\frac{(\mathrm{NIR}-\mathrm{SWIR2})}{(\mathrm{NIR}+\mathrm{SWIR2})}$	SWIR is the reflectance at short wave near-infrared spectral region (2.11-2.29μm) and NIR is the reflectance at Near Infra-red spectral region (0.85-0.88μm)	Hunt and Rock (1989)
9	Surface Albedo	((0.356*B1) + (0.130*B2) + (0.373*B3) + (0.085*B4) + (0.072*B5) -0.018) / 1.016	Surface albedo is an important property of the Earth surface heat budget.It is unitless and has values ranging from 0 to 1.0 depending on the type of land cover.	Smith (2010)

(MSAVI), Normalized Difference Built-up Index (NDBI), Normalized Difference Water Index (NDWI), Normalized Difference Moisture Index (NDMI), and Normalized Difference Infrared Index for Band 7 (NDIIB7) at 30 m spatial resolution of different months for all the stations during the year of 2013 to 2018 using ERDAS Imagine software. After that, all the indices were upscaled at 500 m spatial resolution using the aggregation method to match them with the spatial resolution of MODIS ET. The scaling up of Landsat indices was done by changing pixel size from 30 to 500 metres by aggregation method. Then, linear regression model (multiple linear regression, MLR) and nonlinear regression models (Least Square Support Vector Machine, LS-SVM) were developed to estimate the ET. The MLR and LS-SVM models were developed using upscaled Landsat8 indices (at 500 m resolution) as a predictor variables and MODIS ET (at 500 m resolution) as a predictand variable for the estimation of ET. The developed models are then applied to the nine Landsat indices of 30 m resolution to estimate the ET at 30m scale. The Penman-Monteith (PM) method ET (Allen *et al*., 1998) was used to calculate the station-based ET using observed meteorological data. The correlation coefficient (CC, Boddy and Smith, 2009), Nash-Sutcliffe coefficient (NASH, Nash and Sutcliffe, 1970), Root Mean Square Error (RMSE, Pontious *et al*., 2008) and Normalised Mean Square Error (NMSE, Poli and Cirillo, 1993) were used to estimate the models performance (MLR and LS-SVM). To calculate Landsat ET at 500 m resolution, the developed models were also applied to upscaled indices (at 500 m scale). Again, accuracy assessment was carried out between downscaled ET, MODIS ET and PM ET. ArcGIS 10 was used for database creation, analysis, and map preparation. Further, for statistical and graphical analysis, MATLAB software was used. The details description of MLR, LS-SVM and PM methods can be found in previous research works (Suykens *et al*., 1999; Duhan and Pandey, 2015; Lu *et al*., 2019; Jhajharia *et al*.,

2012; Darshana *et al*., 2013). The brief description of methods used in the present study is described below.

3.1 *Penman-Monteith (PM) method*

The modified Penman-Monteith FAO-56 (Allen *et al*., 1998) was used to calculate reference evapotranspiration (ET_0). It has two important advantages. First, it can be used in a great variety of environments and climate scenarios without any local calibrations due to its physical basis. Second, it is a well-established method that has been validated using lysimeter under a wide range of climate conditions. The main drawback of this method is large number of meteorological parameters required for its application, i.e. air temperatures, relative humidity, wind speed, and solar radiation. The modified Penman-Monteith equation used to calculate the ET_0 are given below:

$$ET_0 = \frac{0.408\Delta(R_n - G) + \gamma \frac{900}{T + 273} u_2 (e_s - e_a)}{\Delta + \gamma(1 + 0.34u_2)}$$

where ET_0 is the reference crop evapotranspiration (mm/day); Δ is the slope of vapor pressure versus temperature curve at temperature T (kPa $°C^{-1}$); γ is the psychrometric constant (kPa $°C^{-1}$); u_2 is the wind speed at a 2 m height (m/s); R_n is the net radiation at crop surface (MJ m^{-2} day^{-1}); G is the soil heat flux density (MJ m^{-2} day^{-1}); T is the average air temperature at 2 m height (°C); $e_s$is the saturation vapor pressure at the temperature of air. e_a is the actual vapour pressure (kPa); (e_s–e_a) is the saturation vapor pressure deficit (kPa). The weather variables used to calculate the parameters of ET_0 are maximum temperature; minimum temperature; relative humidity and wind speed. Moreover, various parameters used in the calculation of ET_0 are actual vapour pressure, vapour pressure deficit, extraterrestrial radiation, net radiation and soil heat flux are calculated using the procedure given by Allen *et al*. (1998).

3.1.1. *Landsat 8 indices estimation*

Surface albedo and vegetation indices were calculated from Landsat 8 OLI surface reflectance. Bands 1-7 surface reflectance was used to calculate vegetation indices and albedo. For generating LST, brightness temperature of band 10 was used (Barsi *et al.*, 2014). Vegetation greenness indices (*i.e*., NDVI, SAVI and MSAVI) were computed by Rause *et al*. (1974), Huete (1988) and Qi *et al.* (1994) algorithm. The vegetation water indices such as NDMI, NDWI, NDIIb7 and NDBI were estimated by the procedure suggested by Wilson and Sader (2002); McFeeters (1996); Hunt and Rock (1989), and Zha *et al.* (2003) in the present study. The Surface Albedo (α) was calculated according to Smith (2010) algorithm. The TIR band 10 was used to estimate the brightness temperature (Xu and Chen, 2004) and vegetation proportion was calculated using the procedure suggested by Wang *et al*. (2015). The algorithm was developed to calculate LST in ERDAS Imagine 2014 software. The metadata, of the satellite-images was used in this algorithm.

3.2. *Aggregation method*

Aggregation is the process of combining several measures into a simpler set of measure. Aggregation of remotely sensed variables becomes more complicated when dealing with the heterogeneity of the land surface (Brunsell and Gillies, 2003) because of the nonlinearity in surface energy balance fluxes at the land atmosphere interface. During the aggregation process, the original spatial data are reduced to a smaller number of data units (less number of pixels) (Bian and Butler, 1999). As a result, each aggregated data unit represents the larger pixel than the original image. The spatial resolution of remotely sensed data and other energy balance fluxes depends on the specification of satellite sensors, which further depends primarily on the scale of the study area to be analyzed. There are three aggregation methods namely averaging, median and central-pixel resampling are commonly used for aggregating in many scientific disciplines. All the methods extract a value over an n by n window in the original image. The windows are adjacent but do not overlap. The averaging method uses the average value over the n by n window. This method may be deemed more appropriate for aggregating remotely sensed images, because a pixel value is assumed to be the integrated value over the corresponding area on the ground. The central pixel resampling method takes the original value of the central pixel of the n by n window. This method is more commonly used in modelling communities such as hydrology (Wolock and Price, 1994). The median method takes the median of the n by n window. This method is perhaps less used in practical works but it is easy to implement and less sensitive to extreme data values. In the present study, the averaging method was used to upscale the 30 m Landsat 8 indices at 500 m resolution. The Landsat 8 data were upscaled at 500 m resolution using the aggregate method which encompasses, filling of 500 m pixel with the average of all the pixel falling within single 500 m pixel of Landsat 8 to match them with MODIS (Bian and Butler, 1999).

3.3. *MLR and LS-SVM model development*

For the development of models (*i.e.*,MLR and LS-SVM) around 70% of data were randomly chosen for training, and the remaining 30% of data were used for

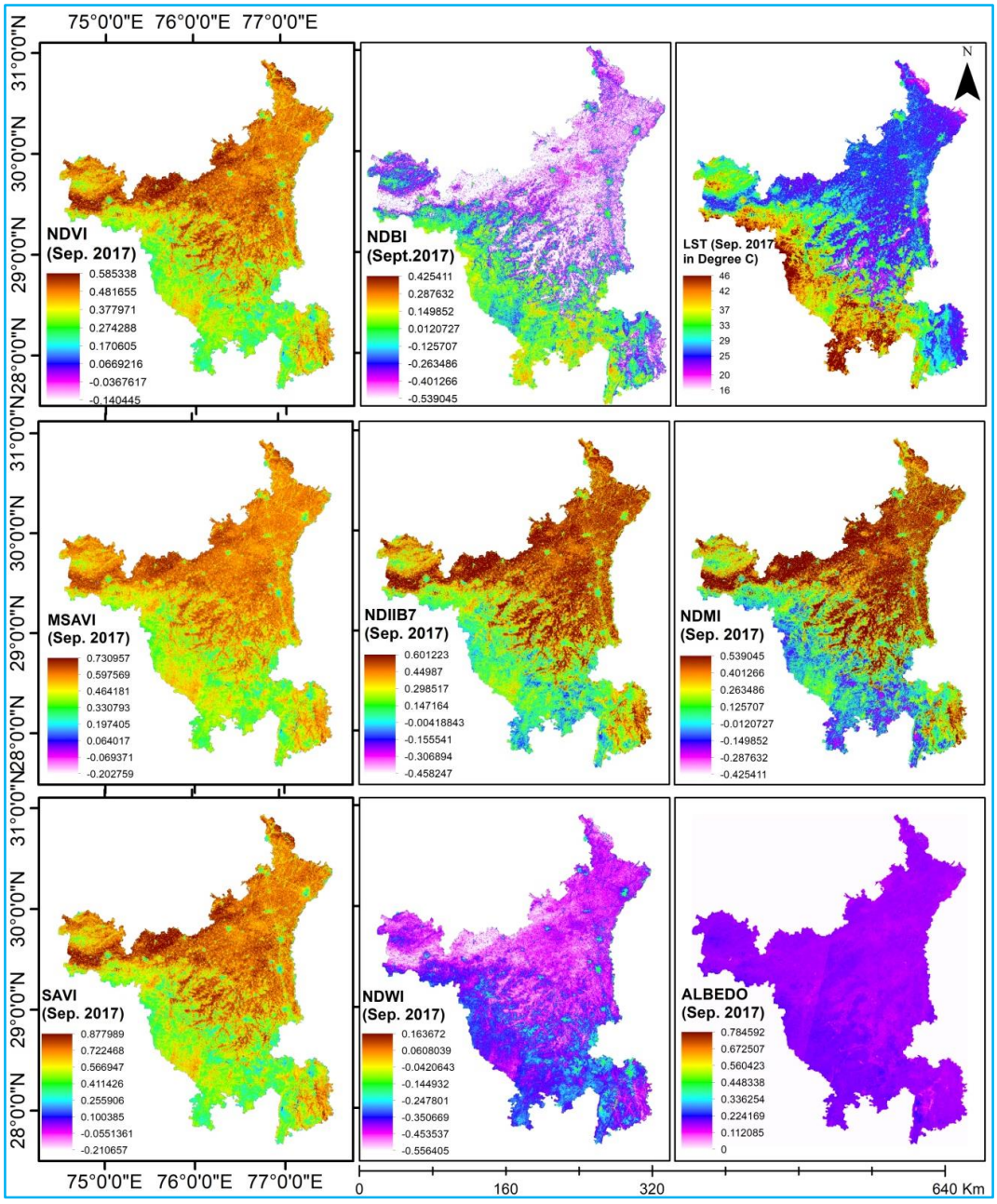

Fig. 3. Spatial map of different indices in the study area during September, 2017

TABLE 5

Results of Sigma and Gamma used for the development of LS-SVM model at different stations

Parameter	Station Name						
	Ambala	Bhiwani	Gurugram	Hisar	Karnal	Narnaul	Rohtak
Sigma	18.92	23.23	1.39	6.55	12.72	35.25	21.64
Gamma	4.81	8.11	4.07	35.03	0.78	19.38	15.18

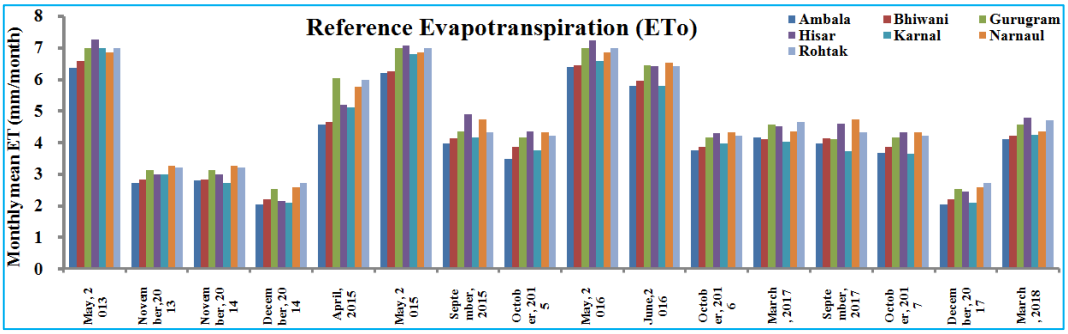

Fig. 4. Monthly variation in ET_0 (mm) using Penman Monteith method

TABLE 6

The developed MLR models for different stations in the study area

Station	Equation
Ambala	$ET_{Ambala} = -36.36 * Albedo + 58.41 * NDVI - 123.01 * SAVI - 11.79 * MSAVI - 20.36 * NDMI - 115.59 * NDWI + 56.45 * NDIIB7 + 0.07 * LST + 13.59$
Bhiwani	$ET_{Bhiwani} = -35.81 * Albedo - 2.20 * NDVI - 34.36 * SAVI - 1.46 * MSAVI - 94.16 * NDMI - 71.36 * NDWI + 66.63 * NDIIB7 - 0.13 * LST + 25.91$
Gurugram	$ET_{Gurugram} = -7.62 * Albedo + 0.23 * NDVI + 9.38 * SAVI - 12.76 * MSAVI + 76.07 * NDBI + 50.43 * NDWI + 57.62 * NDIIB7 + 0.32 * LST + 12.60$
Hisar	$ET_{Hisar} = 58.03 * Albedo - 27.51 * NDVI + 48.01 * SAVI + 9.02 * MSAVI + 78.45 * NDMI + 85.06 * NDWI - 60.94 * NDIIB7 + 0.04 * LST + 13.54$
Karnal	$ET_{Karnal} = -52.67 * Albedo + 5.97 * NDVI - 210.29 * SAVI + 38.80 * MSAVI - 11.16 * NDBI - 249.55 * NDWI + 25.24 * NDIIB7 - 0.04 * LST + 20.60$
Narnaul	$ET_{Narnaul} = -7.34 * Albedo + 8.89 * NDVI - 80.51 * SAVI - 5.32 * MSAVI - 24.71 * NDBI - 109.03 * NDWI + 1.83 * NDIIB7 - 0.04 * LST + 14.14$
Rohtak	$ET_{Rohtak} = -19.03 * Albedo + 2.90 * NDVI - 101.33 * SAVI + 36.51 * MSAVI + 63.39 * NDMI - 110.92 * NDWI - 12.21 * NDIIB7 - 0.003 * LST + 8.44$

testing the model. The data from 2013 to 2016 (around 70%) was used to calibrate the models and remaining (2017 to 2018) were used to validate the models at all the stations in the study area.

The LS-SVM model development needs the "gamma" and squared kernel parameters whose values were derived using the RBF kernel and grid search optimization algorithms as identified the best kernel based on the cost function's minimum value (Duhan and Pandey 2015). LS-SVM development with RBF kernel involves the selection of RBF kernel width gamma and sigma parameter. Table 5 shows the values of sigma and gamma in the study area. The results (Table 5) indicates that maximum sigma value was observed for Narnaul station (35.25) and lowest was recorded at Gurugram station (1.39). Further, the optimal value of gamma was found lowest at Karnal station (0.78) whereas, the maximum value of gamma was recorded at Hisar station (35.03). The optimal values of sigma and gamma were used for training the models. The LS-SVM model training gave the value of α and β for simulating the training values (Sachindra *et al.*, 2013). The model was subject to the above-mentioned process of cross-validation. The MLR and LS-SVM models were developed using MATLAB 2007b.

4. Result and discussion

4.1. *Establishment of Landsat 8 band Indices*

Fig. 3 shows the spatial variations in nine indices during September, 2017 in the study area. The spatial variations are observed throughout the study area. The probable reason for this may be due to the heat waves flow prominently in the region during the months of May and June which leads to increase in temperature. While

TABLE 7

Correlation coefficient between MODIS ET and different indices used for the development of models

S. No.	Station Name	Correlation Coefficient								
		Albedo	LST	MSAVI	NDBI	NDIIB7	NDMI	NDVI	NDWI	SAVI
1.	Ambala	-0.37	0.09	0.11	0.26	0.34	-0.26	0.14	0.03	0.03
2.	Bhiwani	-0.25	0.42	0.27	0.01	0.04	0.01	0.15	0.34	0.26
3.	Gurugram	-0.22	0.20	0.35	0.64	0.49	-0.64	0.06	0.29	0.37
4.	Hisar	-0.14	0.17	0.34	0.07	0.12	-0.07	0.38	0.30	0.34
5.	Karnal	-0.35	0.27	0.49	0.50	0.56	-0.50	0.27	0.52	0.53
6.	Narnaul	-0.27	0.21	0.52	0.18	0.17	-0.18	0.27	0.47	0.53
7.	Rohtak	-0.11	0.35	0.37	0.12	0.09	-0.12	0.32	0.29	0.20

TABLE 8

Results of MLR and LS-SVM models during calibration at different station

S. No.	Station Name	CC		NASH		RMSE		NMSE		R^2	
		LS-SVM	MLR	LS-SVM	MLR	LS-SVM	MLR	LS-SVM	MLR	LS-SVM	MLR
1.	Ambala	0.84	0.89	0.69	0.73	3.78	3.12	0.29	0.25	0.71	0.79
2.	Bhiwani	0.91	0.93	0.81	0.87	2.76	2.23	0.18	0.12	0.83	0.87
3.	Gurugram	0.99	0.97	0.95	0.97	0.41	0.67	0.01	0.03	0.91	0.97
4.	Hisar	0.99	0.90	0.99	0.80	0.70	2.68	0.01	0.18	0.99	0.80
5.	Karnal	0.79	0.75	0.47	0.63	3.20	2.86	0.29	0.34	0.56	0.63
6.	Narnaul	0.93	0.92	0.85	0.85	1.49	1.50	0.14	0.14	0.86	0.85
7.	Rohtak	0.92	0.84	0.83	0.70	2.53	3.31	0.16	0.27	0.84	0.70

cold waves are dominant in December and January months when the lowest temperature take place during these months. Sharma & Joshi (2015) and Mathew *et al.* (2016) found similar results. The results revealed that there is a wide range of variations in vegetation and water indices throughout the year at different locations which may be considered enough for representing largely all the vegetation existing in the State. Variations in these indices values due to the reason that during the study time land was fallow after the harvesting of crops and thus led to an increase in the temperature. Moreover, once the south-west monsoon season comes it leads to an increase in the vegetation cover of the land and thereby increasing values during that period (Rawat *et al.*, 2017). The indices values were found to be affected by type and density of vegetation, soil texture, and the prevailing climatic conditions during the season. The indices values were changed due to high temperature, low water availability and vegetation condition during the growing season (Das *et al.*, 2017). As the vegetation cover is very low because of absence of crops and rainfall which usually arrives during monsoon season, *i.e.*, 1st week of June, therefore, there is no additional source of moisture/irrigation during the month of May leading lower values of indices.

4.2. *Reference Evapotranspiration (ET_0)*

The monthly mean ET_0 calculated using FAO56 Penman-Monteith was shown in Fig. 4 during the year 2013 to 2018. The graph depicts that ET_0 was lowest in the month of December while in it was maximum in the month of May in the year of 2018. The probable reason for the maximum ET_0 during the month of May is due to highest temperature during this month and other local prevailing climatic conditions. The reverse trend was observed in the month of December, which recorded the minimum ET_0 value because the temperature remains low during this month as compared to other months of the

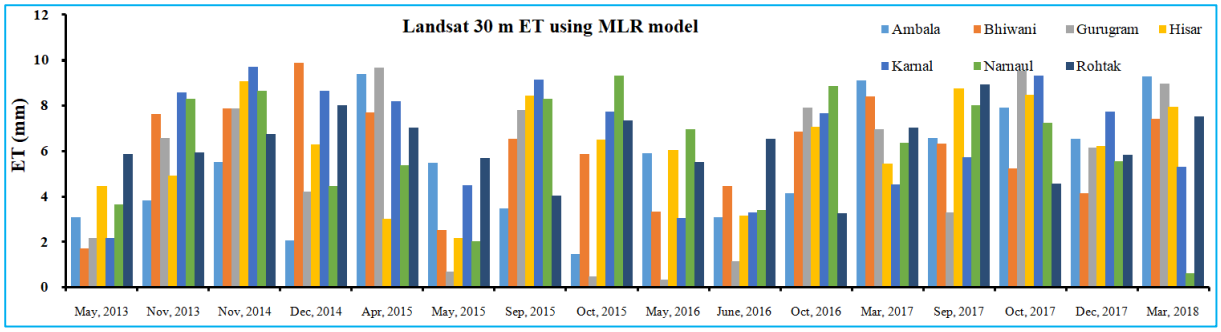

Fig. 5. Landsat 30 m ET using MLR model for all stations

TABLE 9

Results of MLR and LS-SVM models during validation at different station in the study area

S. No.	Station Name	CC		NASH		RMSE		NMSE		R^2	
		LS-SVM	MLR	LS-SVM	MLR	LS-SVM	MLR	LS-SVM	MLR	LS-SVM	MLR
1.	Ambala	0.91	0.75	0.67	-2.68	12.46	41.88	0.07	2.76	0.82	0.56
2.	Bhiwani	0.85	0.42	0.66	-1.60	15.59	43.37	0.02	1.95	0.73	0.18
3.	Gurugram	0.99	0.54	0.99	-0.01	0.01	10.16	0.01	0.76	0.99	0.29
4.	Hisar	0.99	0.51	0.99	-0.57	0.01	14.37	0.01	1.18	0.99	0.26
5.	Karnal	0.85	0.40	0.47	-4.35	2.71	8.65	1.88	4.01	0.72	0.16
6.	Narnaul	0.91	0.52	0.65	-1.37	10.25	26.79	0.02	1.78	0.83	0.27
7.	Rohtak	0.91	0.26	0.70	-0.20	5.21	10.47	0.16	0.90	0.82	0.07

year. Again, with respect to different locations/stations, the highest ET was observed at Hisar station because it is the hottest station in the study area.

4.3. *Model development*

The developed MLR model for different station namely; Ambala, Bhiwani, Gurugram, Hisar, Karnal, Narnaul and Rohtak are shown in Table 6. To identify the effect of different indices on ET, correlation coefficient was calculated and shown in Table 7. The results of correlation coefficient between MODIS ET (at 500 m resolution) and different indices (at 500 m resolution) represent the weightage given to each index derived from Landsat data for the estimation of ET. The results show a negative correlation between ET and Albedo, NDMI, NDVI & SAVI. However, LST, MSAVI, NDBI, NDIIB7 and NDWI show a positive correlation with ET. To assess which parameters affect the ET at most, the correlation coefficient using all the data of different stations were also calculated (Table 7). From the results, it is found that SAVI (CC = -0.73) followed by NDVI (CC = -0.72), NDIIB7 (CC = 0.72), NDWI (CC = 0.69), MSAVI (CC = 0.64), NDBI (CC = 0.64), LST (CC = 0.64), NDMI (CC = -0.58) and Albedo (CC = -0.44). It may be concluded from the above results that SAVI, NDVI and NDIIB7 indices are highly correlated with MODIS ET.

4.4. *Comparison between MLR and LS-SVM model*

The performance of developed models was analyzed by using performance indicators, *i.e.*, CC, NASH, RMSE, NMSE and R^2 during calibration and validation. The calibration and validation were performed using MOD16A2 ET and estimated ET at 500 m resolution. The models which give the highest CC, R^2& NASH and lowest RMSE &NMSE are considered the best models (Duhan, *et al.*, 2021).

During calibration (Table 8), CC ranged from 0.79 (Karnal station) to 0.99 (Hisar & Gurugram station) for LS-SVM model while for MLR it varies from 0.75 (Karnal station) to 0.99 (Hisar station). For LS-SVM model, the NASH varied from 0.47 (Karnal station) to 0.99 (LS-SVM) between different stations. It ranged from 0.63 (Karnal station) to 0.97 (Gurugram station) for MLR

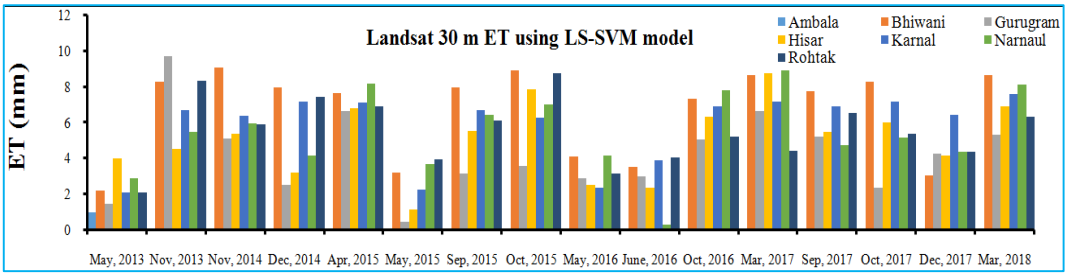

Fig. 6. Landsat 8 30 m ET using LS-SVM model for all stations

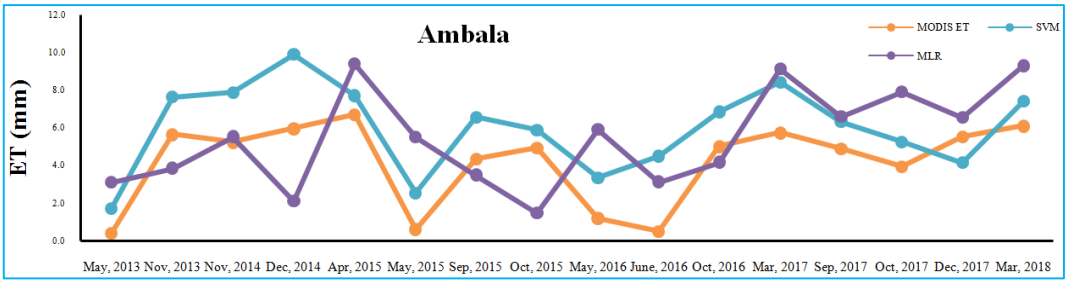

Fig. 7. Comparison of different model for Ambala station

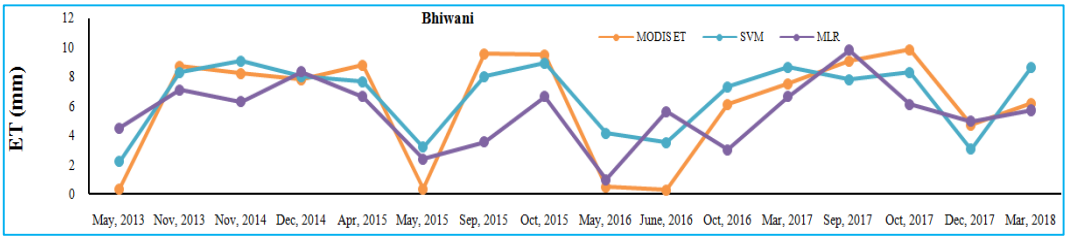

Fig. 8. Comparison of Different model for Bhiwani station

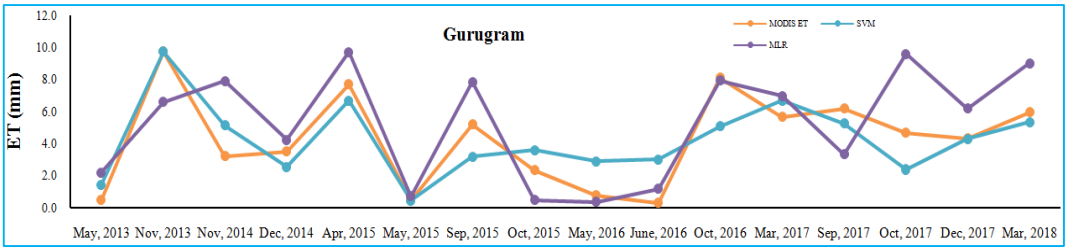

Fig. 9. LST Comparison of Different model for Gurugram station

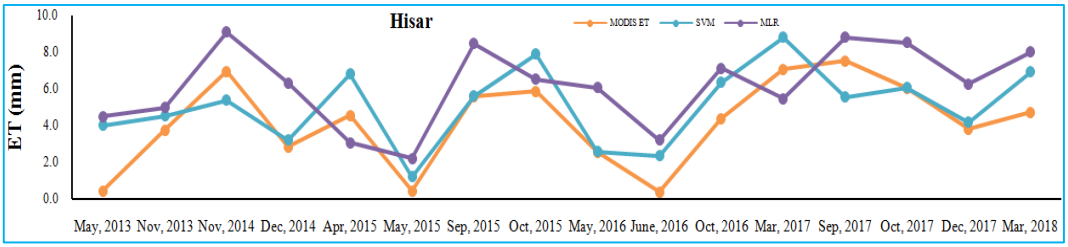

Fig. 10. Comparison of different model for Hisar station

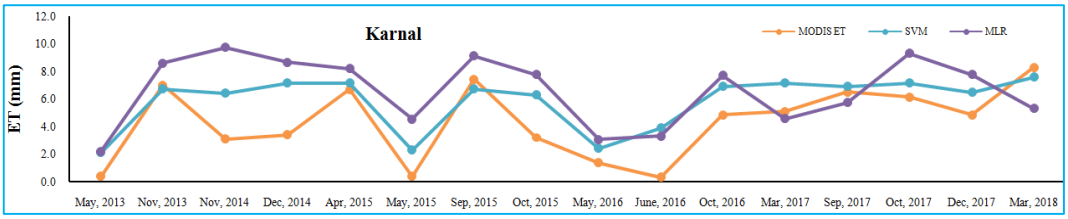

Fig. 11. Comparison of different model for Karnal station

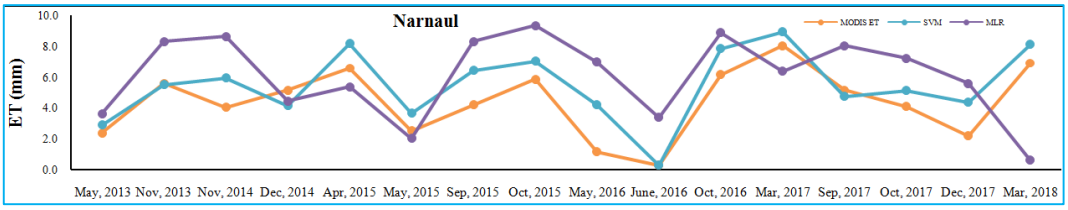

Fig. 12. Comparison of different model for Narnaul station

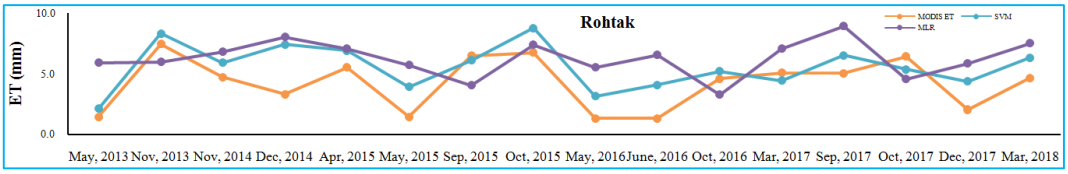

Fig. 13. Comparison of Different model for Rohtak station

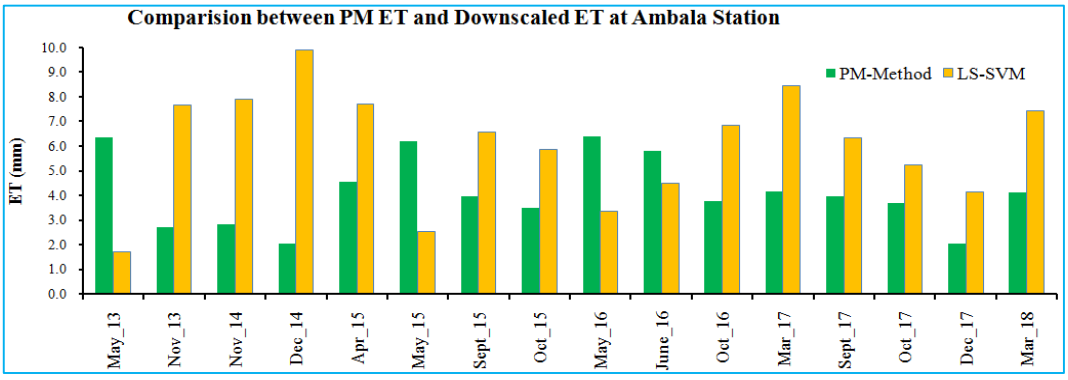

Fig. 14. Comparison between PM method ET and Downscaled ET for Ambala station

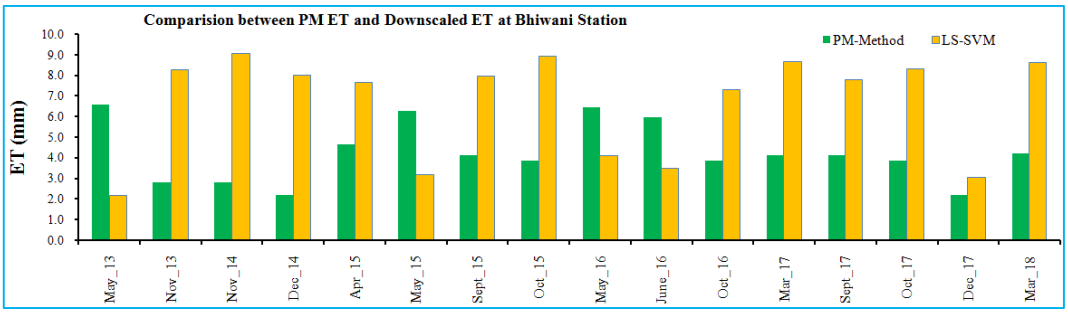

Fig. 15. Comparison between PM method ET and Downscaled ET for Bhiwani station

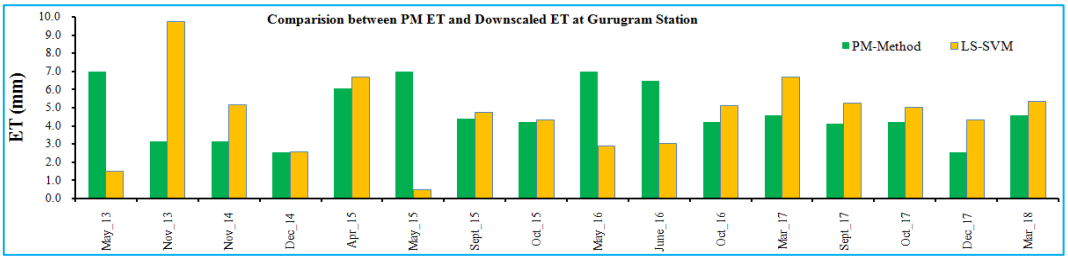

Fig. 16. Comparison between PM method ET and Downscaled ET for Gurugram station

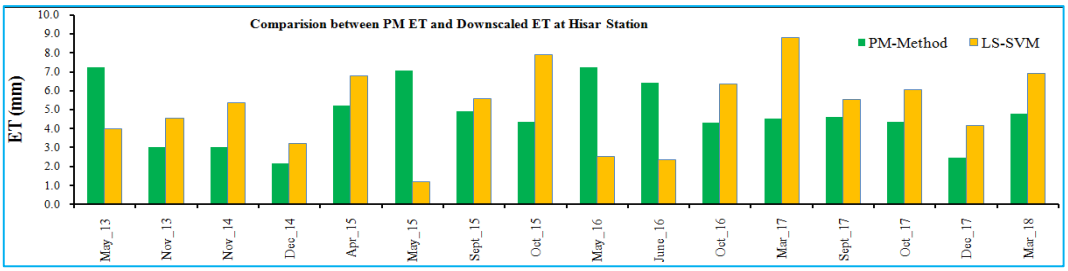

Fig. 17. Comparison between PM method ET and Downscaled ET for Hisar station

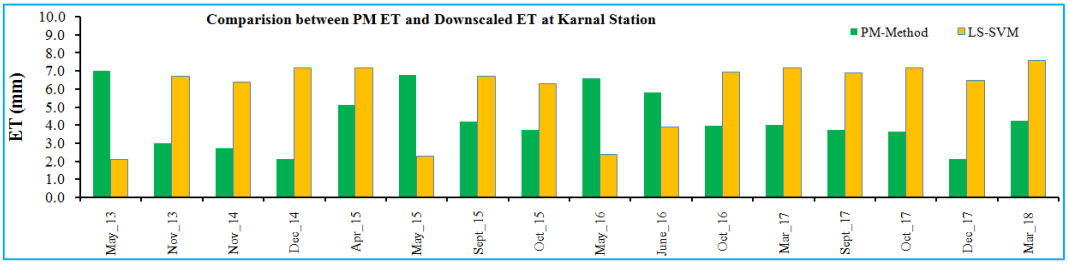

Fig. 18. Comparison between PM method ET and Downscaled ET for Karnal station

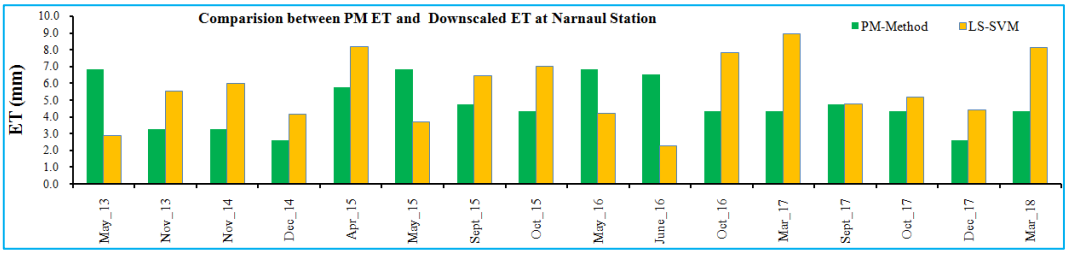

Fig. 19. Comparison between PM method ET and Downscaled ET for Narnaul station

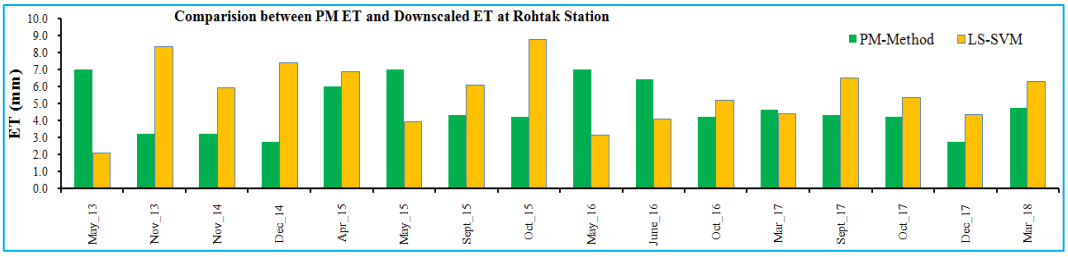

Fig. 20. Comparison between PM method ET and Downscaled ET for Rohtak station

TABLE 10

Correlation coefficient between models for different stations

Station	Correlation coefficient		
	LS-SVM & MODI	MLR & MODI	MLR & LS-SVM
Ambala	0.89	0.11	0.02
Bhiwani	0.80	0.49	0.55
Gurugram	0.98	0.90	0.90
Hisar	0.98	0.65	0.66
Karnal	0.71	0.50	0.36
Narnaul	0.84	0.52	0.66
Rohtak	0.86	0.64	0.77

model. The RMSE for calibration varies from 0.41 (Gurugram station) to 3.78 (Ambala station) for LS-SVM model whereas it varies from 0.67 (Gurugram station) to 0.31 (Rohtak station) for MLR model. The lowest NMSE was found at Hisar & Gurugram stations (0.01) and highest was observed at Karnal station (0.29) for LS-SVM model. For MLR model, it was found highest for Karnal station (0.34) and lowest for Gurugram station (0.03).

During validation (Table 9), CC ranged from -0.75 to 0.54 for MLR model and from 0.85 to 0.99 for LS-SVM model between different stations. The lowest and highest NASH was -4.35 and -0.01 for MLR model while for LS-SVM, lowest and highest NASH efficiency observed was 0.47 and 0.99. The RMSE for the validation period ranged from 8.65 to 41.88 for MLR model and it varies from 0.001 to 15.59 for LS-SVM models between different stations. For LS-SVM model, the lowest and highest NMSE was 0.01 and 1.88 while for MLR, it was found from 0.76 to 4.01. In addition, R^2 ranged from 0.07 to 0.56 for MLR model and from 0.72 to 0.99 for LS-SVM model among different stations. The maximum values of CC, NASH and R^2 and the minimum value of RMSE and NMSE during calibration and validation showed that the LS-SVM model slightly outperformed than MLR model. Similar results were reported by other researchers also (Duhan and Pandey, 2015; Pham *et al*., 2019; Sachindra *et al*., 2013 and Tripathi *et al*., 2006).

4.5. *Estimation of ET estimates using MLR and LS-SVM model*

The ET calculated by employing MLR and LS-SVM models is shown in Figs. 5 and 6 respectively using Landsat 30 m indices. ET calculated using MLR model was highest for Bhiwani station and lowest for Gurugram station. This may be due to that Bhiwani is located in semi-arid region which is a water scarcity and scanty vegetation area as compared to other stations. The estimated ET (Fig. 6) using LS-SVM model of different stations clearly indicates that the lowest value was found for Karnal station while highest was observed at Bhiwani station in the study area. The highest value of ET may be due to the high temperature in this region (Singh and Bala, 2012; Rawat *et al.*, 2017).

4.6. *Results of ET estimation by MODIS, LS-SVM and MLR model*

The variations were observed in MODIS ET, LS-SVM ET and MLR ET for different stations namely; Ambala, Bhiwani, Gurugram, Hisar, Karnal, Narnaul and Rohtak (Figs. 7 to 13). A perusal of results presented in Figs. 7 to 13 indicates that ET calculated by LS-SVM model has a similar trend as MODIS. Unlike LS-SVM, ET trend by MLR model found varying from MODIS for different stations. The comparison shows that the LS-SVM performs well in ET estimation as compared to the MLR, at fine resolution (Duhan and Pandey, 2015 and Goyal *et al*., 2014). Lin *et al*. (2013) also found that SVM based model is superior to multilayer perception models for ET pan estimation due to its accuracy, robustness and efficiency. Duhan & Pandey (2015) stated that LS-SVM is the best model among multiple linear regression (MLR), ANN and LS-SVM. Results demonstrated that the MODIS ET product is compatible with downscaled ET overall and shows detailed spatial and temporal variation trend with a resolution of 30 m.

4.7. *Correlation between calculated and simulated ET*

The correlation coefficient was computed between ET obtained from MODIS, LS-SVM and MLR at different stations namely Ambala, Bhiwani, Gurugram, Hisar,

Karnal, Narnaul, and Rohtak and results are shown in Table 10. The result shows a significant correlation between MODIS ET and LS-SVM ET at all the stations. The lowest value of R^2 was found at Karnal station while Gurugram and Hisar stations show maximum value. The lowest correlation was observed between MODIS ET and MLR ET. Ke *et al.* (2015) also reported that the correlation between MODIS ET and LS-SVM model ET is good as compared to another model. Duhan and Pandey (2015) are also found the similar performance of the LS-SVM model as compared to the MLR model.

4.8. *Comparison between PM ET method and downscaled ET*

The comparison between downscaled ET at 30 m scale using LS-SVM model and PMET showed a similar trend at all stations (Figs. 14 to 20). The downscaled model overestimates ET in comparison to the PM method. A similar finding was reported by Hu *et al.* (2015). The reason behind the overestimation could be the spatial differences at the different stations and heterogeneity of land cover and the built-up area around stations (Ke *et al.*, 2015). Presence of plant foliage and buildings around the observatory for instruments might be affecting the downscaled ET pixel that is covered by vegetation and built-up area (Mahour *et al.*, 2017). The downscaled LS-SVM ET has a good agreement with MODIS ET. A comparable temporal trend was seen between downscaled ET, MODIS ET and PM ET.

5. Conclusion

The estimation of evapotranspiration at finer temporal and spatial scale greatly assists in the planning, evaluation, development and management of water resources. This research is aimed to generate 30 m ET using Landsat 8 dataset from MODIS 500 m ET. In the present study, the downscaling models (*i.e.*, LS-SVM and MLR) were developed for the estimation of ET at 30 m scale using Landsat 8 data. Nine indices namely SAVI, NDVI, MSAVI, NDWI, NDMI, NDIIb7, Surface Albedo, LST and NDBI are calculated from Landsat 8 data. The models are then developed using Landsat indices (at 500 m scale) as a predictor variables and MODIS 8-day 500 m ET (MOD16A2) as a response variable. The calibration and validation results indicated that both the developed models are good models for the ET estimation, however, LS-SVM model outperformed the MLR model at all stations. It was depicted from the results that MODIS ET had a good agreement with downscaled Landsat ET. A comparable temporal trend was shown by the downscaled ET using LS-SVM model and MODIS ET. From the finding, it can be concluded that LS-SVM model has a great potential and capability for downscaling ET at finer scale. Further, finding also suggests that SAVI, NDVI and NDIIB7 indices are highly correlated with MODIS ET. This study may be helpful for water resource managers, planners and agricultural scientists.

Disclaimer : The contents and views expressed in this study are the views of the authors and do not necessarily reflect the views of the organizations they belong to.

References

Aiazzi, B., Alparone, L., Baronti, S. and Garzelli, A., 2002, "Context-driven fusion of high spatial and spectral resolution images based on oversampled multi resolution analysis", *IEEE Transactions on geoscience and remote sensing*, **40**, 10, 2300-2312.

Allen, R. G., Pereira, L. S., Raes, D. and Smith, M., 1998, "Crop evapotranspiration-Guidelines for computing crop water requirements-FAO Irrigation and drainage paper 56", *Fao, Rome*, **300**, 9, D05109.

Allen, R. G., Pereira, L. S., Raes, D. and Smith, M., 1998, "Crop Evapotranspiration", Guidelines for Computing Crop Water Requirements, FAO Irrigation and Drainage, Paper No. 56. FAO, Rome.

Anderson, Ray G., Yufang Jin, Y., Michael L. and Goulden, M. L., 2012, "Assessing regional evapotranspiration and water balance across a Mediterranean montane climate gradient", *Agricultural and Forest Meteorology*, **166-167**, 10-22.

Barsi, J., Schott, J., Hook, S., Raqueno, N., Markham, B. and Radocinski, R., 2014, "Landsat-8 thermal infrared sensor (TIRS) vicarious radiometric calibration", *Remote Sensing*, **6**, 11, 11607-11626.

Bian, L., and Butler, R., 1999, "Comparing effects of aggregation methods on statistical and spatial properties of simulated spatial data", *Photogrammetric Engineering and Remote Sensing*, **65**, 73-84.

Blaney, H. F. and Criddle, W. D., 1950, "Determining Water Requirements in Irrigated Areas From Climatological and Irrigation Data", Soil Conservation Service Technical Paper 96, Soil Conservation Service. US Department of Agriculture, Washington.

Boddy, R. and Smith, G. L., 2009, "Statistical methods in practice: for scientists and technologists", Chichester, UK: Wiley; 95-96.

Brunsell, N. A. and Gillies, R. R., 2003, "Scale issues in land-atmosphere interactions: Implications for remote sensing of the surface energy balance", *Agricultural and Forest Meteorology*, **117**, 3, 203-221.

Darshana, D., Pandey, A. and Pandey, R. P., 2013, "Analyzing trends in reference evapotranspiration and weather variables in the Tons River Basin in Central India", *Stochastic Environmental Research and Risk* Assessment, **27**, 1407-1421.

Darshana and Ashish, P., 2012, "Long-term Trends in Rainfall Pattern over Haryana, India", *International Journal of Research in Chemistry and Environment*, **2**, 1, 283-292.

Das, P. K., Sahay, B., Seshasai, M. V. R. and Dutta, D., 2017, "Generation of improved surface moisture information using angle-based drought index derived from Resourcesat-2 AWiFS for Haryana state, India", *Geomatics, Natural Hazards and Risk*, **8**, 2, 271-281.

Duhan, D. and Pandey, A., 2015, "Statistical downscaling of temperature using three techniques in the Tons River basin in Central India", *Theoretical and applied climatology*, **121**, 3-4, 605-622.

Duhan, D., Singh, D. and Arya, S., 2021, "Effect of projected climate change on potential evapotranspiration in the semiarid region of central India". *Journal of Water and Climate Change*, **12**, 5, 1854-1870.

Goyal, M. K., Bharti, B., Quilty, J., Adamowski, J. and Pandey, A., 2014, "Modeling of daily pan evaporation in sub-tropical climates using ANN, LS-SVR, Fuzzy Logic, and ANFIS", *Expert Systems with* Applications, **41**, 11, 5267-5276.

Goyal, R. K., 2004, "Sensitivity of evapotranspiration to global warming : a case study of arid zone of Rajasthan (India)", *Agricultural Water Management*, **69**, 1, 1-11.

Hansen, V. E., Israelsen, O. W. and Stringham, G. E., 1980, "Irrigation principles and practices", John Wiley & Sons, New York.

Hargreaves, G. L. and Samani, Z. A., 1985, "Reference crop evapotranspiration from temperature", *Applied Engineering in Agriculture*, **1**, 2, 96-99.

Hong, S. H., Hendrickx, J. M. and Borchers, B., 2011, "Down-scaling of SEBAL derived evapotranspiration maps from MODIS (250 m) to Landsat (30 m) scales", *International journal of Remote Sensing*, **32**, 21, 6457-6477.

Hu, G., Jia, L. and Menenti, M., 2015, "Comparison of MOD16 and LSA-SAF MSG evapotranspiration products over Europe for 2011", *Remote Sensing of Environment*, **156**, 510-526.

Huete, A. R., 1988, "A soil-adjusted vegetation index (SAVI)", *Remote sensing of Environment*, **25**, 3, 295-309.

Hunt Jr, E. R. and Rock, B. N., 1989, "Detection of changes in leaf water content using near-and middle-infrared reflectances", *Remote Sensing of Environment*, **30**, 1, 43-54.

Jhajharia, D., Dinpashoh, Y., Kahya, E., Sing, V. P. and Fakheri-Fard, A., 2012, "Trends in reference evapotranspiration in the humid region of northeast India", *Hydrological Processes*, **26**, 421-435.

Ke, Y., Im, J., Lee, J., Gong, H. and Ryu, Y., 2015, "Characteristics of Landsat 8 OLI-derived NDVI by comparison with multiple satellite sensors and *in-situ* observations", *Remote Sensing of Environment*, **164**, 298-313.

Ke, Y., Im, J., Park, S. and Gong, H., 2016, "Downscaling of MODIS One kilometer evapotranspiration using Landsat-8 data and machine learning approaches", *Remote Sensing*, **8**, 3, 215.

Knipper, K., Hogue, T., Scott, R. and Franz, K. 2017, "Evapotranspiration estimates derived using multi-platform remote sensing in a semiarid region", *Remote Sensing*, **9**, 3, 184.

Kumar, D., Arvind, Nain, A. J., Singh, A., Mor, A. and Sushant Bhardwaj, S., 2021, "Geo-spatial technology application for prioritization of land resources in Udham Singh Nagar District of Uttarakhand, India", *Indian Journal of Traditional Knowledge*, **20**, 2, 595-603.

Kumar, D., Arvind, Nain, A. J., Singh, Darshana, Arya, S., Bhardwaj, S., and Abhilash, 2019, "Soil loss estimation using geo-spatial technology in north western trai region of India", *Journal of Agrometeorology*, **21**, 1, 182-188.

Liang, S., Zhao, X., Yuan, W., Liu, S., Cheng, X., Xiao, Z., Zhang, X., Liu, Q., Cheng, J., Tang, H., Qu, Y. H., Bo, Y., Qu, Y., Ren, H., Yu, K. and Townshend, J., 2013, "A Long-term Global LAnd Surface Satellite (GLASS) Dataset for Environmental Studies", *International Journal of Digital Earth*, **6**, 5-33.

Lin, G. F., Lin, H. Y. and Wu, M. C., 2013, "Development of a support vector-machine-based model for daily pan evaporation estimation", *Hydrological Processes*, **27**, 22, 3115-3127.

Lu, Y., Yin, Q., Li, H., Sun, H., Yang, Y. and Hou, M., 2019, "The LS-SVM algorithms for boundary value problems of high-order ordinary differential equations", *Advances in Difference Equations*, **1**, 195.

Mahour, M., Tolpekin, V., Stein, A. and Sharifi, A., 2017, "A comparison of two downscaling procedures to increase the spatial resolution of mapping actual evapotranspiration", *ISPRS Journal of Photogrammetry and Remote Sensing*, **126**, 56-67.

Mathew, A., Khandelwal, S. and Kaul, N., 2016, "Spatial and temporal variations of urban heat island effect and the effect of percentage impervious surface area and elevation on land surface temperature: Study of Chandigarh city, India", *Sustainable Cities and Society*, **26**, 264-277.

McFeeters, S. K., 1996, "The use of the Normalized Difference Water Index (NDWI) in the delineation of open water features", *International Journal of Remote Sensing*, **17**, 7, 1425-1432.

Monteith, J. L., 1965, "Evaporation and environment", *Symposia of the Society for Experimental Biology*, **19**, 205-224.

Nash, J. E. and Sutcliffe, J. V., 1970, "River flow forecasting through conceptual models part I-A discussion of principles", *Journal of Hydrology*, **10**, 3, 282-290.

Niaghi A. R., Oveis Hassanijalilian, O. and Jalal Shiri, J., 2021, "Estimation of Reference Evapotranspiration Using Spatial and Temporal Machine Learning Approaches", *Hydrology*, **8**, 1,25.

Penman, H. L., 1948, "Natural evaporation from open water, bare soil and grass", *Proceedings of the Royal Society of London Series A – Mathematical and Physical Sciences*", **193**, 1032, 120-145.

Pham, Q. B., Yang, T. C., Kuo, C. M., Tseng, H. W. and Yu, P. S., 2019, "Combing Random Forest and Least Square Support Vector Regression for Improving Extreme Rainfall Downscaling", *Water*, **11**, 3, 451.

Poli, A. A. and Cirillo, M. C., 1993, "On the use of the normalized mean square error in evaluating dispersion model performance", *Atmospheric Environment. Part A General Topics*, **27**, 15, 2427-2434.

Pontious, Jr., R. G., Thontteh, O. and Chen, H., 2008, "Components of information for multiple resolution comparison between maps that share a real variable", *Environmental and Ecological Statistics*, **15**, 2, 111-142.

Priestley, C. H. B. and Taylor, R. J., 1972, "On the assessment of surface heat flux and evaporation using large-scale parameters", *Monthly Weather Review*, **100**, 81-82.

Qi, J., Chehbouni, A., Huete, A. R., Kerr, Y. H., and Sorooshian, S., 1994, "A modified soil adjusted vegetation index", *Remote Sensing of Environment*, **48**, 2, 119-126.

Rawat, K. S., Bala, A., Singh, S. K., and Pal, R. K., 2017, "Quantification of wheat crop evapotranspiration and mapping: A case study from Bhiwani District of Haryana, India", *Agricultural Water Management*, **187**, 200-209.

Rouse, J. W, Haas, R.H., Schell, J. A. and Deering, D. W., 1974, "Monitoring vegetation systems in the Great Plains with ERTS", *Proceedings of the Third Earth Resources Technology Satellite (ERTS) Symposium, Vol 1. Washington D.C. NASA S.P.*-351, 309-317.

Sachindra, D. A., Huang, F., Barton, A., and Perera, B. J. C., 2013, "Least square support vector and multilinear regression for statistically downscaling general circulation model outputs to catchment streamflows", *International Journal of Climatology*, **33**, 5, 1087-1106.

Sharma, R. and Joshi, P. K., 2015, "The Changing Urban Landscape and Its Impact on Local Environment in an Indian Megacity: The Case of Delhi", In *Urban Development Challenges, Risks and Resilience in Asian Mega Cities* (61-81). Springer, Tokyo.

Singh, D., Singh, R., Anurag, Shekhar, C., Rao, V. and Singh, S., 2010, "Agroclimatic Atlas of Haryana", Technical Bulletin No. 15, Department of Agricultural Meteorology, CCSHAU, Hisar. p80.

Singh, R. K. and Bala, A., 2012, "Monitoring of evapotranspiration in major districts of Haryana using Penman Monteith method", *International Journal of Engineering Science and Technology*, **4**, 7,

Smith, R. B., 2010, "The heat budget of the earth's surface deduced from space", Yale University Center for Earth Observation: New Haven, CT, USA.

Suykens, J. A. K., Lukas, L., Van Dooren, P., De Moor, B. and Vandewalle, J., 1999, "Least squares support vector machine classifiers: a large scale algorithm", In *European Conference on Circuit Theory and Design, ECCTD*, **99**, 839-842.

Tan, S., Wu, B., Yan, N., and Zhu, W., 2017, "An NDVI-based statistical ET downscaling method" *Water*, **9**, 12, 995.

Thornthwaite, C. W., 1948, "An approach toward a rational classification of climate", *Geographical Review*, **38**, 55-94.

Tripathi, S., Srinivas, V. V. and Nanjundiah, R. S., 2006, "Downscaling of precipitation for climate change scenarios: a support vector machine approach", *Journal of hydrology*, **330**, 3-4, 621-640.

Wang, F., Qin, Z., Song, C., Tu, L., Karnieli, A. and Zhao, S., 2015, "An improved mono-window algorithm for land surface temperature retrieval from Landsat 8 thermal infrared sensor data", *Remote Sensing*, **7**, 4, 4268-4289.

Wang, F., Qin, Z., Song, C., Tu, L., Karnieli, A. and Zhao, S., 2015, "An improved mono-window algorithm for land surface temperature retrieval from Landsat 8 thermal infrared sensor data", *Remote Sensing*, **7**, 4, 4268-4289.

Wang, L., Kisi, O., Hu, B., Bilal, M., Zounemat-Kermanie, M. and Hui Lia, H., 2017, "Evaporation modeling using different machine learning techniques", *International Journal of* Climatology, **37**, 1076-1092.

Wilson, E. H. and Sader, S. A., 2002, "Sensing of Environment", **80**, 3, 385-396.

Wolock, D. M. and Price, C. V., 1994, "Effects of digital elevationmodel map scale and data resolution on a topography-based watershed model", *Water Resources Research*, **30**, 11,3041-3052.

Xu, H. Q., and Chen, B. Q., 2004, "Remote sensing of the urban heat island and its changes in Xiamen City of SE", *Journal of Environmental Sciences*, **16**, 2, 276-281.

Yang, Y., Sun, H., Xue J., Liu, Y., Liu, L., Yan, D. and Gui, D., 2021, "Estimating evapotranspiration by coupling Bayesian model averaging methods with machine learning algorithms", *Environmental Monitoring and Assessment*, **3**;193(3), 156.

Yao, Y., Liang, S., Li, X., Chen, J., Liu, S., Jia, K., Zhang, X., Xiao, Z., Fisher, J.B., Mu, Q., Pan, M., Liu, M., Cheng, J., Jiang, B., Xie, X., Grünwald, T., Bernhofer, C. and Roupsard, O., 2017, "Improving global terrestrial evapotranspiration estimation using support vector machine by integrating three process-based algorithms", *Agricultural and Forest Meteorology*, **242**, 55-74.

Zha, Y., Gao, J. and Ni, S., 2003, "Use of normalized difference built-up index in automatically mapping urban areas from TM imagery", *International journal of remote sensing*, **24,** 3, 583-594.